J Mater Sci (2026) 61:3315–3324

Materials for life sciences

Tailoring biodegradable polymer mechanics for biomedical use: in situ nanobeam WAXS analysis of poly(ester amide) and poly(ester urea)

N. Zavradashvili[1], A. Davydok[2], R. Katsarava[1], and S. Grigorian[3,*]

[1] *Institute of Chemistry and Molecular Engineering, Agricultural University of Georgia, Kakha Bendukidze University Campus, # 240 David Aghmashenebeli Alley, 0159 Tbilisi, Georgia*
[2] *Institute of Materials Physics, Helmholtz Zentrum Hereon, Notkestr 85, 22607 Hamburg, Germany*
[3] *Department of Physics, University of Siegen, Walter-Felx-Str 3, 57068 Siegen, Germany*

Received: 30 July 2025
Accepted: 14 December 2025
Published online: 4 January 2026

ABSTRACT

Biodegradable pseudo-proteins (PPs), a novel class of synthetic polymers mimicking natural proteins, offer unique advantages for biomedical applications, including superior biocompatibility, tuneable degradation, and structural versatility. In this study, we investigate the mechanical and microstructural behavior of two representative PPs—poly(ester amide) (PEA) and poly(ester urea) (PEU)—using a novel in situ stretching technique combined with nanobeam wide-angle X-ray scattering (WAXS). This advanced methodology enables real-time, submicron-resolution analysis of molecular ordering during mechanical deformation. For both PEA and PEU, the WAXS patterns two distinguished (001) and (010) peaks associated with lamellar stacking and chain–chain packing of aliphatic segments, correspondingly. Our results reveal that PEA, characterized by higher crystallinity of the (010), exhibits brittle fracture under stress, whereas PEU demonstrates elastic behavior due to its lower (010) crystalline content and greater chain mobility. These findings establish a direct correlation between sectional crystallinity and mechanical performance, providing valuable insights for the rational design of PPs with tailored properties for biomedical use.

Introduction

In recent years, the development of biodegradable polymers (BPs) has been one of the leading frontiers in the construction of new biomaterials for sophisticated medical applications. The biodegradation leads to debris that can get to be dissolvable or metabolizable, and ultimately are cleared from the body. BPs utilized for biomedical purposes must have acceptable properties from the view point of biocompatibility, processability, sterilization capability, and shelf life [1]. Among the naturally occurring BPs proteins

Handling Editor: Steven Naleway.

Address correspondence to E-mail: grigorian@physik.uni-siegen.de

https://doi.org/10.1007/s10853-025-12060-5

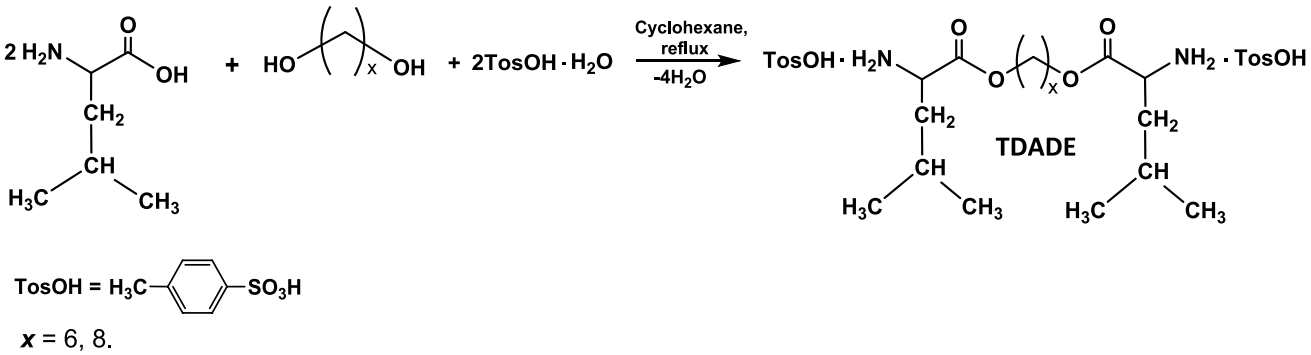

Scheme 1 The structure of TDADEs – key monomers for synthesizing PPs *(TDADEs used in the study are provided).*

occupy a leading position—they are suitable for both surgical and pharmaceutical applications due to their innate affinity to tissues, enzymatic biodegradability with release of α-amino acids (α-AAs) that could be assimilated by the organism, thus promoting tissue regeneration [2–4]. A new generation of α-AA-based BPs, called "pseudo-proteins" (PPs), is synthetic polymers designed to mimic the structure and function of natural proteins. Unlike traditional proteins, which consist of α-AAs linked by peptide bonds in a head-to-tail orientation, PPs often have alternative linkages, such as tail-to-tail or head-to-head connections. This unique architecture imparts distinct properties to these biomimetic materials, making them valuable for a wide range of applications and are increasingly utilized in numerous end use industries and sectors such as biomedicine, cosmetics, agriculture, as well as food processing, preservation, and packaging, as eco-friendly materials [5–9].

PPs have important advantageous characteristics over both synthetic and naturally occurring BPs such as polyesters and proteins. One of the main advantages of the PPs over polyesters (such as polyglycolide—PGA, polylactide—PLA—and their copolymers, and polycaprolactone) is much better tissue compatibility [6, 8]. Another important advantage of PPs as biomaterials consists in more favorable local pH drop in tissues after biodegradation that can cause lower irritation of tissues. Additional advantages are synthesis under normal atmospheric conditions at moderate temperatures, widest range of desirable material properties, longer shelf life, solubility in common organic solvents and alcohols, excellent adhesion to many surfaces that is important for applications as coatings, tunable in a wide-ranging balance of hydrophobicity/hydrophilicity, to name a few [5–7]. PPs possess positive features of proteins such as a high tissue compatibility and a nutritive potential for cells. At the same time, PPs are free of the limitations of proteins: no batch-to-batch variation, no risk of disease transmission, a wide range of tunable material properties, and low to zero immune reaction.

Bis-(α-amino acid)-alkylene diesters (diamine diesters, DADEs) are key bis-nucleophilic monomers for synthesizing virtually unlimited number of PPs—representatives of a huge family of ester polymers known as having reasonable biodegradation rates through the hydrolysis of ester moieties [7–9]. DADEs are composed of cheap and vastly available components such as AAs, diols and *p*-toluenesulfonic acid (Scheme 1). They are synthesized as stable di-*p*-toluenesulfonic acid salts (TDADEs) via very simple and cost-effective procedure—direct thermal condensation of two moles of α-amino acids with one mole of diols in the presence of two moles of *p*-toluenesulfonic acid [10–12]. The TDADEs are synthesized in high yields (up to 90–95%). Additional merits of the TDADE monomers are their purification by recrystallization from the cheapest solvent—water, stability upon storage and highly active terminal amino groups for successful chain growth along with the designed-in non-proteinaceous ("head-to-head") orientation of amino acids, enzyme-specific lateral groups R, and labile (hydrolysable) ester bonds (Scheme 1) that goes later into macromolecules made of them. The TDADEs are the universal bis-nucleophilic monomers which, after interacting with various bis-electrophiles (cholrides or active diesters) [7–9, 12], lead to the synthesis of three basic classes of the PPs such as poly(ester amide)s (PEAs), poly(ester urea)s (PEUs), and poly(ester urethane)s

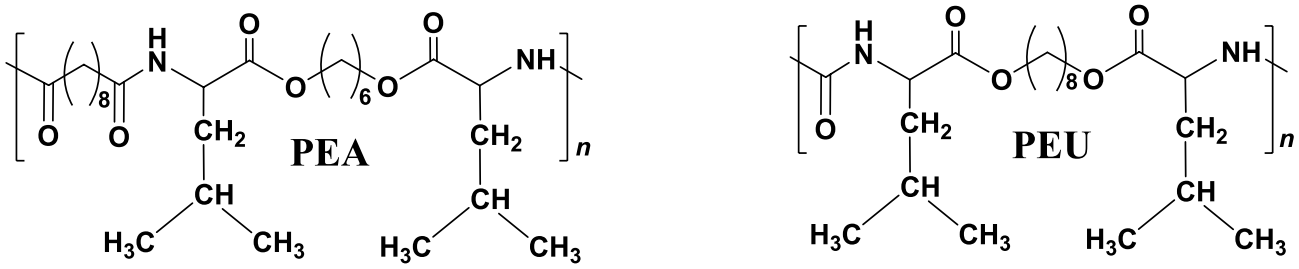

Scheme 2 Chemical structures of the synthesized PEA (8L6) and PEU (1L8).

(PEURs). The TDADEs are highly attractive monomers from chemical, technological, economical, and ecological points of view [10–13, 20].

As a result of numerous experiments, it was found that, taking into account the availability and price of raw materials, the wide range of polymer properties, the most promising classes of PPs are PEAs and PEUs. Among α-amino acids, L-leucine (price, biological and physicochemical properties of the obtained PP, etc.) is considered the best, among diols—1,6-hexamethylene diol—and among diacids—sebacic acid (for synthesis of PEAs) and carbonic acid (for synthesis of PEUs) [14–19].

The proposed work presents an in-depth investigation of the physico-mechanical properties of polymeric materials (PPs) [21]. In particular, we studied the morphology of representatives from two classes—PEA and PEU—using optical microscopy and synchrotron-based x-ray techniques [22, 23]. A central aspect of the study is the use of a novel in situ stretching setup based on wide-angle x-ray scattering (WAXS) with a nanobeam, which is essential for probing internal structure and molecular ordering in polymers—key factors that influence their physical and mechanical behavior [24]. This methodology enabled us to reveal distinct structural responses of PEA and PEU under deformation [25]. The approach offers valuable insights into the structure, morphology, and mechanical stability of these emerging polymer systems and holds potential for extension to other PP materials [26]. This methodological approach builds upon and extends the framework of previous studies in reflection geometry on semiconducting polymers under mechanical load [27]. A central innovation in this study is the implementation of a novel in situ tensile deformation setup integrated with nanobeam WAXS in transmission geometry which enables localized probing of molecular ordering and strain-induced structural changes at submicron resolution. This method is essential for studying the anisotropic mechanical responses and phase behavior of semicrystalline and amorphous polymer domains under uniaxial stress—factors that are critical for applications requiring mechanical durability and functional stability.

Materials and methods

Two classes of PPs—poly(ester amide) (PEA) and poly(ester urea) (PEU)—were synthesized using the interfacial polycondensation (IP) method, as previously reported [12]. The IP reaction was performed at room temperature in a biphasic system consisting of a hydrophobic organic solvent (dichloromethane, DCM) and water. Sodium carbonate was used as an acceptor of p-toluenesulfonic acid (TosOH) and hydrochloric acid (HCl), both of which are released during the condensation reaction. The PEA (8L6) and PEU (1L8) polymers were synthesized using key bis-nucleophilic monomers, namely TDADEs (Scheme 1): bis-(L-leucine)-1,6-hexylene diester di-p-toluenesulfonate (L6) and bis-(L-leucine)-1,8-octylene diester di-p-toluenesulfonate (L8). Sebacoyl chloride (SC) served as the bis-electrophilic monomer for synthesizing PEA (8L6), whereas triphosgene (TP) was used as the bis-electrophilic monomer for synthesizing PEU (1L8).

The chemical structures of the resulting polymers are given in Scheme 2. The synthesized PEA and PEU were purified by re-precipitation from ethanol into distilled water, followed by filtration and drying under reduced pressure at 50 °C until constant weight was achieved.

The main characteristics of the synthesized polymers are summarized in Table 1. Molecular weights were estimated by GPC (Waters Associates, Inc.,

Table 1 Basic properties of the synthesized PPs

#	Structure	Yield, %	Molecular weight characteristics		Solubility** (0.1 g in 1 mL)			
1	PEA—8L6	96	68,400	1.79	+	+	+	+
3	PEU—1L8	97	146,600,	1.65	+	+	+	+

Milford, United States. Styragel columns in DMF: HR4, HR3, HR0.5 all 7.8 × 300 mm) equipped with a high-pressure liquid chromatography pump (Waters 1525 Binary HPLC) and a Waters refractive index detector 2414 and UV detector (Waters 2487 dual absorbance detector, = 240 nm). A solution of LiBr (0.1 M) in dimethylformamide (DMF) was used as an eluent (flow rate 1.0 mL/min). The Mw and Mw/Mn were calculated using PEG standards; ** Solubility: "+"—soluble at r.t.

Optical and Synchrotron measurements

The surface morphology of both samples was examined using a 3D laser scanning optical microscope (VK-X3000, Keyence, Japan), which combines confocal and white light interferometry techniques to capture high-resolution topographical data.

Synchrotron x-ray measurements were taken at the Nanofocus Endstation of the P03 beamline at PETRA III, DESY (Hamburg, Germany) [28]. The photon energy was set to 16.7 keV, and the X-ray beam was focused to a spot size of approximately 1.5 × 1.5 μm^2 using Kirkpatrick–Baez (KB) mirrors provided by JTEC Corporation. The scattered X-ray signal was collected using a Dectris Eiger 9 M detector with a pixel size of 75 × 75 μm^2, positioned 388 mm downstream from the sample.

We have employed the wide-angle x-ray scattering (WAXS) which is a powerful technique used to probe the molecular and crystalline structure of materials, particularly polymers and soft matter. When applied in transmission geometry, the x-rays pass through the sample, enabling structural analysis of thin films with minimal background interference (see Fig. 1). Here the x-rays are directed perpendicularly onto the thin film, and the scattered signal is detected on the opposite side by a Dectris Eiger 9 M detector. In the context of this miniature experimental setup, several key features are notable: This stretching mode is optimal for thin films and enabling high signal-to-noise ratios for structural features in the nanometer range.

A custom tensile stage is integrated into the x-ray beam path where the configuration enables high-resolution structural analysis at the nanoscale. The thin film is mounted in the stage and stretched uniaxially while WAXS patterns are collected stepwise for the given stretching steps up to 100% strain. This setup

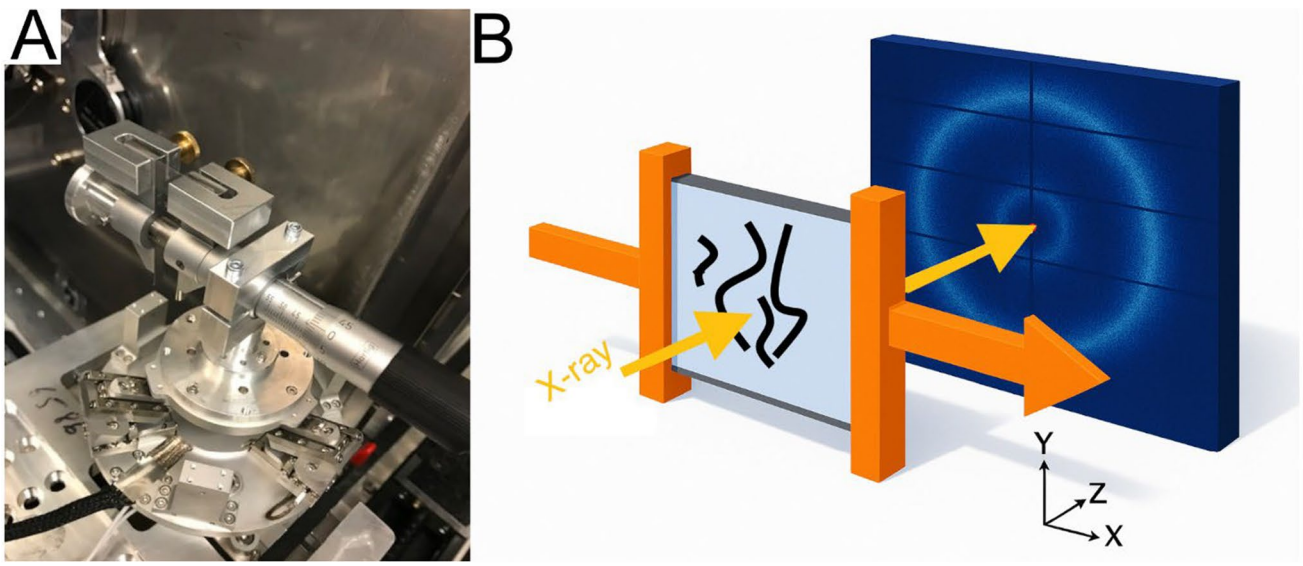

Figure 1 Miniature setup for WAXS measurements of thin films using a focused nanobeam.

ensures displacement-controlled measurements, where the film is stretched incrementally. At each step, the strain is increased to a predefined value and then held constant during WAXS data acquisition.

Measurements were taken in a single-shot mode at various stages of uniaxial stretching, with each exposure lasting 60 s. After each acquisition, the sample position was vertically shifted by 20 μm to avoid beam-induced damage from prior measurements. The collected diffraction data were processed using the pyFAI module for azimuthal (1D) integration [29], followed by analysis and visualization using custom MATLAB scripts developed in-house.

Results and discussion

Prior to the in situ stretching experiments combined with X-ray scattering, the thickness and morphology of the samples were examined using optical microscopy. The thicknesses of the PEU and PEA films were found to be 233.9 μm and 267.7 μm, respectively. Figure 2 presents the surface morphology of the samples, with color coding from blue to red indicating the progression from the lowest to the highest regions. A clear distribution of molecular domains is visible across the sample surfaces. For both samples, the typical height of these domains is approximately 400 nm, as indicated by the red arrows. However, a significant difference in domain density is observed: The PEU sample exhibits nearly twice the domain density compared to the PEA sample. The displayed field of view is representative of the entire sample surface for both cases. These morphological differences motivated further investigation of the structural and mechanical properties through in situ stretching tests coupled with X-ray scattering analysis.

X-ray diffraction analysis was employed to investigate the changes in crystalline structure of PEA and PEU polymers under varying levels of mechanical stretching. The applied strain values were precisely correlated with wide-angle X-ray scattering (WAXS) measurements to assess corresponding microstructural changes. Representative 2D WAXS images for both materials are shown in Figs. 3A and B. The polymers exhibit structural behavior dependent on urea segment content and their processing history, with PEA demonstrating different distribution of the crystallinity than PEU, primarily due to the enhanced molecular packing facilitated by amide linkages and their strong intermolecular hydrogen bonding. To ensure accurate interpretation, background scattering was subtracted to minimize experimental artifacts, and a 60° vertical integration sector ("cake") was used for analysis. The resulting scattering patterns in both polymers display two concentric rings, indicating periodic structural features on two distinct length scales. The symmetry of these rings suggests an absence of preferred orientation in the sample. Additionally, the one-dimensional line profiles derived from azimuthal

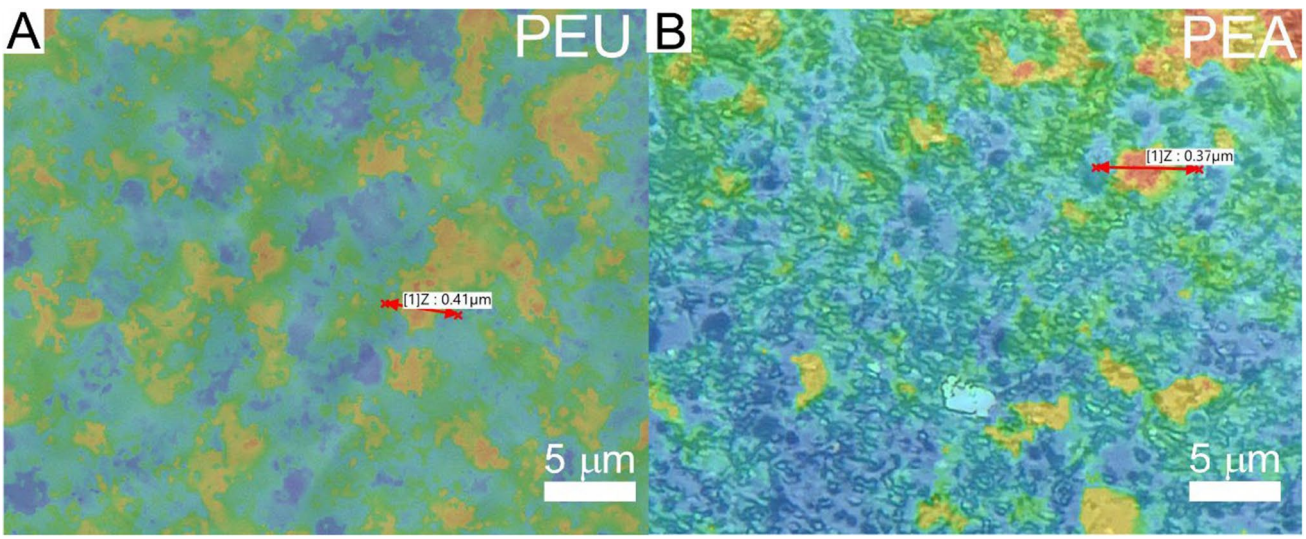

Figure 2 Optical microscope images of the surface of **A** PEU sample and **B** PEA sample.

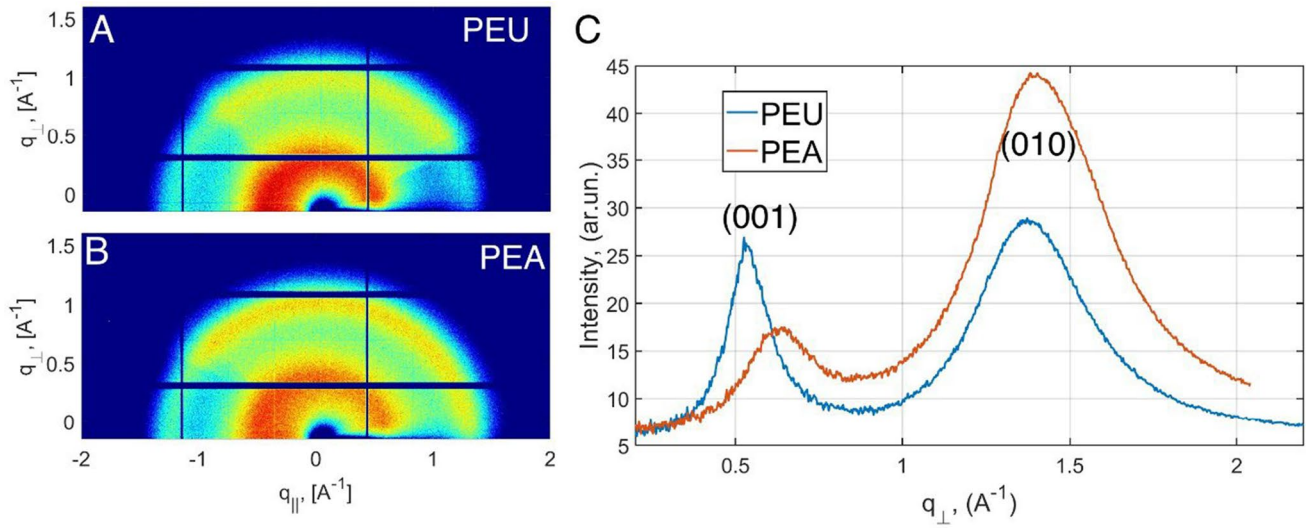

Figure 3 Initial 2D WAXS patterns of PEU **A** and PEA **B** C—integrated curves of PEU and PEA signals.

integration Fig. 3C reveal distinct differences in scattering intensity between PEU and PEA, further highlighting their structural dissimilarities.

For both PEU and PEA materials, only two distinct peaks are observed in the low- and high-Q ranges. In the absence of multiple peaks in the WAXS patterns, we propose that both materials have a liquid crystalline-like structure. Similarly, two broad peaks were found in the X-ray diffraction pattern of a melt-spun PEA fiber [35]. In the case of large crystals prepared by isothermal crystallization, the PEA became more ordered and was assigned to an orthorhombic unit cell [35]. Further on XRD analysis was used to study how the crystalline structure changes under various stretching steps [30]. The mechanical strain values are precisely linked with the WAXS measurements and correlated with microstructural changes [31]. 2D WAXS images of PEU and PEA polymers show that both polymers exhibit behavior dependent on the urea segment content and polymer processing history [32]. PEA is more crystalline than PEU due to better packing from amide linkages, which promote strong intermolecular hydrogen bonding [33, 34].

The first (100) peak, located at lower Q is associated with the chain folding, mainly determined by methylene packing and side group spacing (lamellar stacking). The second (010) peak at higher Q-values correspond to the corresponds to chain–chain packing of aliphatic segments, similar to monoclinic-like polyethylene-type or poly(ester urea)s packing [35, 36]. For the PEU film the (100) and (010) peaks appear of comparable intensity. The first (100) peak, located at Q = 0.51 $Å^{-1}$, exhibits a relatively narrow full width at half maximum (FWHM) of 0.25 $Å^{-1}$. The (001) peak corresponds to a characteristic real-space distance of 12.27 Å. The broader (010) peak at Q = 1.36 $Å^{-1}$ has a FWHM of 0.34 $Å^{-1}$, corresponding to a spacing of 4.60 Å. In the case of the PEA material, similar dual-peak behavior is observed; however, the position and intensity of the peaks differ from those of PEU. The lower-Q (100) peak for PEA is shifted toward higher Q, appearing at Q = 0.63 $Å^{-1}$, which corresponds to a shorter real-space periodicity of 9.95 Å. This peak is nearly half as intense as the analogous peak in the PEU sample and displays a narrower FWHM of 0.13 $Å^{-1}$. Conversely, the higher-Q (010) peak in the PEA sample is significantly more intense than both its corresponding (001) peak and the (010) peak in PEU. It appears at Q = 1.38 $Å^{-1}$, with a FWHM of 0.33 $Å^{-1}$, corresponding to a spacing of 4.54 Å. These results suggest that PEA and PEU exhibit a hierarchical structure, with a distinct distribution of periodicities and relative domain populations.

The observed structural differences between PEU and PEA are expected to have a direct impact on their macroscopic properties, particularly mechanical performance, which is critical for future applications. To gain further insight into the mechanical behavior, an in situ uniaxial stretching experiment was conducted. The experimental setup enabled controlled deformation, with precise measurements of the elongation relative to the initial sample length.

X-ray scattering patterns were recorded at key deformation stages—0%, 50%, and 100% strain. However, in the case of the PEA material, mechanical failure occurred before reaching full extension, with the maximum attainable strain limited to 83.2%. The results are presented in Fig. 4 for the (001) and (010) planes. Integrated scattering profiles at each deformation stage are shown for PEU and PEA in Figs. 4A and 4B, respectively.

We evaluated the degree of crystallinity for PEU and PEA using WAXS data. Crystallinity was determined by calculating the ratio of the integrated area under the crystalline peaks to the total scattering area, which includes both crystalline peaks and the amorphous background. Based on this analysis, we estimated the degree of crystallinity to be similar for both films: 27.6% for PEA and 30% for PEU, respectively. This figure remained almost unchanged upon stretching. Interestingly, the fractions of crystallinity associated with the (001) and (010) planes are different. For the PEU, the (010) contribution is four times higher, whereas for the PEA, it is one order of magnitude higher. This makes a major contribution to crystallinity for the PEA.

Notably, the PEU material successfully withstood stretching up to 100% without failure, whereas the PEA sample fractured at 83% strain, indicating a lower mechanical robustness. The structural evolution under mechanical load was characterized by tracking the position of the most intense scattering peak throughout the deformation process. A summary of this analysis is provided in Fig. 4C for both the (001) and (010) peaks. For both materials, the (001) can accommodate higher strains (up to one order of magnitude higher) than the (010) indicating overall flexibility of the (001) planes. Remarkably the strain for the (010) is rather low, whereas for PEU, the continuous shift of the (010) peak position with increasing strain indicates elastic behavior and progressive alignment or compression of structural domains. In contrast, the PEA material exhibited signs of plastic deformation as early as 50% strain, as evidenced by a plateau in the peak shift, suggesting structural reorganization and the onset of irreversible deformation. These observations highlight the distinct mechanical responses of the two materials, rooted in their underlying nanostructural organization. Taken together optical and X-ray results, these findings demonstrate that the higher domain density

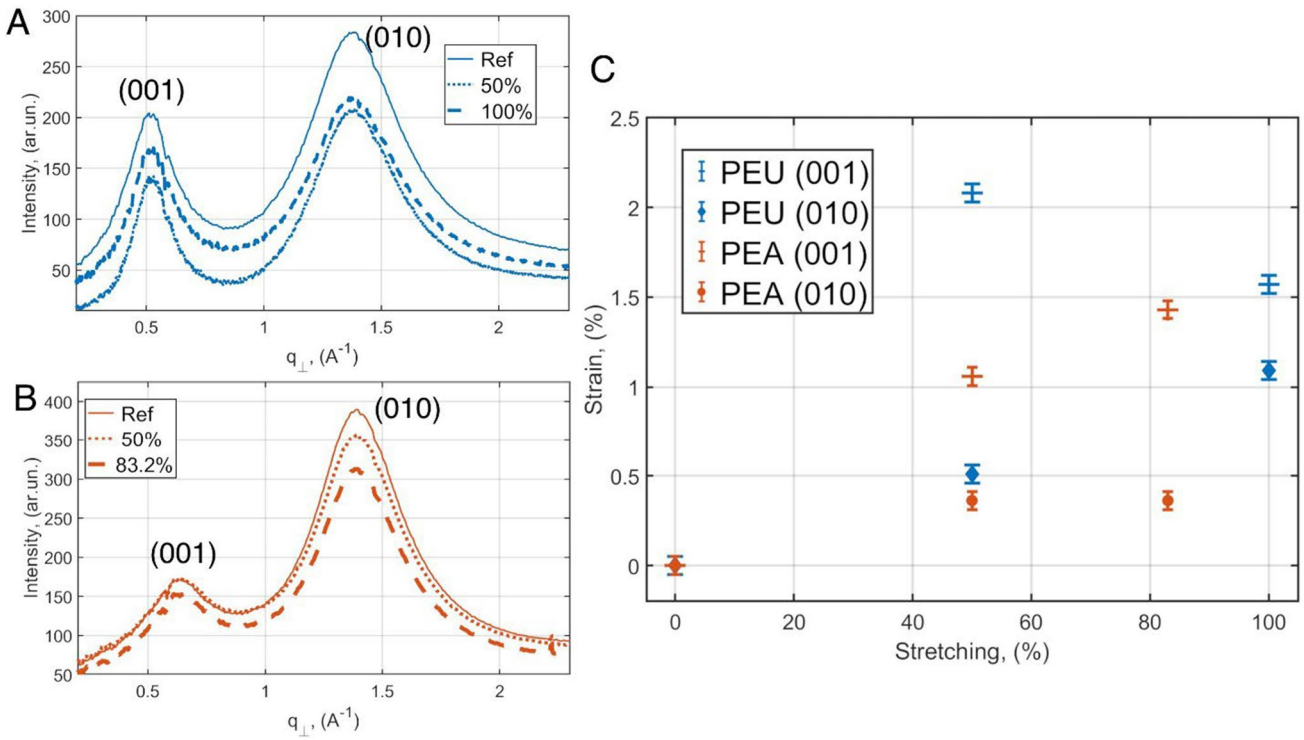

Figure 4 Integrated line profiles of the PEU **A** and the PEA **B** samples as a function of strain, strain-stretching behavior of the PEU (blue) and the PEA (red) samples **C**, correspondingly.

and more uniform morphology observed in PEU contribute to its enhanced mechanical stability and structural resilience under load, underscoring the critical role of nanostructural organization in determining the functional properties of these materials.

Conclusions

The application of a unique stretching WAXS setup with a nanobeam has provided valuable insights into the microstructural behaviors of the PEA and the PEU under mechanical deformation. The PEA exhibits higher (010) crystallinity, contributing to its brittle behavior upon stretching. The well-ordered crystalline regions restrict molecular mobility, leading to fracture under stress. In contrast, the PEU, demonstrates elastic behavior where the increased crystalline content of the (001) allows for greater chain mobility, enabling the material to deform and recover without breaking. During stretching, the PEA's crystalline regions rigidity limits the material's ability to accommodate strain, resulting in brittleness. For applications requiring flexibility and resilience, materials with a lower fraction of the (010) to degree of crystallinity, like the PEU, are preferable. The nanobeam WAXS technique has elucidated the relationship between the fractional crystallinity and mechanical behavior in the PEA and the PEU. Understanding these correlations is crucial for designing biomedical PPs with specific performance characteristics, particularly in fields where mechanical flexibility or rigidity is paramount.

Acknowledgements

The authors acknowledge DESY, Hamburg, for the allocated experiment at the Nanofocus Endstation of the P03 beamline at PETRA III, Volkswagen Foundation, for initiation of cooperation between the Agricultural University of Georgia and the University of Siegen.

Author Contributions

S.G. and R.K. were responsible for conceptualization, resources, and supervision; S.G. and N.Z. assisted with methodology; A.D. helped with software and data curation; A.D. and S.G. were involved in formal analysis, investigation, and writing—review and editing; N.Z. and R.K. took part in writing—original draft preparation; and A.D. and N.Z. participated in visualization. All authors have read and agreed to the published version of the manuscript.

Funding

Open Access funding enabled and organized by Projekt DEAL. Funding for this study was received from the Volkswagen Foundation.

Data availability

The datasets used and/or analyzed during the current study are available from the corresponding author on reasonable request.

Declarations

Conflicts of interest The authors declare no conflicts of interest.

References

[1] Vasanthi K (2017) Biodegradable polymers - a review. Polym Sci 3:1–7

[2] Wosicka-Frąckowiak H, Poniedziałek K, Woźny S, Kuprianowicz M, Nyga M, Jadach B, Milanowski B (2024) Collagen and its derivatives serving biomedical purposes: a review. Polymers 16(18):2668
[3] Choi SM, Chaudhry P, Zo SM, Han SS (2018) Advances in protein-based materials: from origin to novel biomaterials. Adv Exp Med Biol 1078:161–210
[4] Katchalski E, Poly (amino acids): achievements and prospects. In Peptides, polypeptides, and proteins—proceedings of the Rehovot symposium on poly (amino acids), polypeptides, and proteins and their biological implications (Wiley, New York, 1974), pp. 1–13.
[5.] Díaz A, Katsarava R, Puiggalí J (2014) Synthesis, properties and applications of biodegradable polymers derived from diols and dicarboxylic acids: from polyesters to poly(ester amide)s (review). Int J Mol Sci 15:7064–7123
[6] Katsarava R, Kulikova N, Puiggalí J (2016) Amino acid based biodegradable polymers – promising materials for the applications in regenerative medicine (review). J J Regener Med 1(1):012
[7] Zavradashvili N, Puiggali J, Katsarava R (2020) Artificial polymers made of a-amino acids – Poly(Amino Acid)s, Pseudo-Poly(Amino Acid)s, Poly(depsipeptide)s, and Pseudo-Proteins. Curr Pharm Des 26(5):566–593
[8] Yousefzade O, Katsarava R, Puiggalí J (2020) Biomimetic Hybrid Systems for Tissue Engineering. Biomimetics 5:49
[9] Katsarava R, Ten K, Kobauri S (2021) Pseudo-proteins and related synthetic amino acid based polymers (Review). J Mater Educ 43(1–2):33–80
[10] Arabuli N, Tsitlanadze G, Edilashvili L, Kharadze D, Goguadze T, Beridze V, Katsarava R (1994) Heterochain polymers based on natural amino acids. Synthesis and enzymatic hydrolysis of regular poly (ester amide) s based on bis (L-phenylalanine) α, ω-alkylene diesters and adipic acid. Macromol Chem Phys 195(6):2279–2289
[11] Gomurashvili Z, Kricheldorf HR, Katsarava R (2000) Amino acid based bioanalogous polymers. Synthesis and study of new poly (ester amide) s composed of hydrophobic α-amino acids and dianhydrohexitoles. J Macromol Sci Pure Appl Chem 37:215–227
[12] Katsarava R, Gomurashvili Z. (2011). Biodegradable polymers composed of naturally occurring α-amino acids in Handbook of Biodegradable Polymers - Isolation, Synthesis, Characterization and Applications. Ed. By Lendlein A, Sisson A (Wiley-VCH, Weinheim, 2011) p.107.
[13] Memanishvili T, Zavradashvili N, Kupatadze N, Tugushi D, Gverdtsiteli M, Torchilin VP, Wandrey Ch, Baldi L, Manoli SS, Katsarava R (2014) Arginine-based biodegradable ether-ester polymers with low cytotoxicity as potential gene carriers. Biomacromol 15(8):2839–2848
[14] Díaz A, del Valle L, Rodrigo N, Casas M, Chumburidze G, Katsarava R, Puiggalí J (2018) Antimicrobial activity of poly (ester urea) electrospun fibers loaded with bacteriophages. Fibers 6(2):33
[15] Kantaria T, Kantaria T, Kobauri S, Ksovreli M, Kachlishvili T, Kulikova N, Tugushi D, Katsarava R (2016) Biodegradable nanoparticles made of amino-acid-based ester polymers: preparation, characterization, and in vitro biocompatibility study. Appl Sci 6(12):444
[16] Kantaria T, Kantaria T, Heiduschka P, Eter N, Tugushi D, Katsarava R (2023) Dexamethasone-loaded pseudo-protein nanoparticles for ocular drug delivery: evaluation of drug encapsulation efficiency and drug release. J Nanotechnol 1:8827248
[17] Ksovreli M, Kachlishvili T, Mtiulishvili T, Dzmanashvili G, Batsatsashvili T, Zurabiani K, Tughushi D, Kantaria T, Nadaraia L, Rusishvili L, Piot O (2023) Leucine-based pseudo-proteins (LPPs) as promising biomaterials: a study of cell-supporting properties. Polymers 15(15):3328
[18] Zavradashvili N, Jokhadze G, Gverdtsiteli M, Otinashvili G, Kupatadze N, Gomurashvili Z, Tugushi D, Katsarava R (2013) Amino acid based epoxy-poly (ester amide) s - a new class of functional biodegradable polymers: synthesis and chemical transformations. J Macromol Sci Part A: Pure Appl Chem 50(5):449–465
[19] Makharadze D, Kantaria T, Yousef I, Del Valle LJ, Katsarava R, Puiggalí J (2024) PEGylated micro/nanoparticles based on biodegradable poly (ester amides): preparation and study of the core–shell structure by synchrotron radiation-based FTIR microspectroscopy and electron microscopy. Int J Mol Sci 25(13):6999
[20] Zavradashvili N, Sarisozen C, Titvinidze G, Otinashvili G, Kantaria T, Tugushi D, Puiggali J, Torchilin VP, Katsarava R (2019) Library of cationic polymers composed of polyamines and arginine as gene transfection agents. ACS Omega 4(1):2090–2101
[21] Ward IM, Sweeney J. An Introduction to the Mechanical Properties of Solid Polymers, 3rd Edn (Wiley, London, 2012). https://doi.org/10.1002/9781119967125
[22] Stribeck N (2007) X-Ray Scattering of Soft Matter. Springer, Berlin, Heidelberg
[23] Rueda DR (2016) Morphological characterization of segmented polymers by advanced microscopy and synchrotron radiation techniques. Polym Test 50:267–275
[24] Li C, Müller AJ, Zhang Y, Wang T (2015) Nanobeam waxs for in-situ structural investigation of polymer deformation. Macromol Rapid Commun 36(18):1572–1577
[25] Chen W, Kumar S (2016) Mechanically induced structural evolution in segmented copolymers studied by synchrotron X-ray scattering. Polymer 98:376–384

[26] Spano FC, Nguyen TQ, Li J, Smith RA (2018) Correlating morphology and mechanical properties in semicrystalline polymers using advanced X-ray techniques. Macromolecules 51(12):4784–4794
[27] Aliouat MY, Escoubas S, Benoudia MC, Ksenzov D, Duché D, Bènevent E, Videlot-Ackermann C, Ackermann J, Thomas O, Grigorian S (2020) In situ measurements of the structure and strain of a π-conjugated semiconducting polymer under mechanical load. J Appl Phys 127:045108
[28] Krywka C, Keckes J, Storm S, Buffet A, Roth SV, Döhrmann R, Müller M (2013) Nanodiffraction at MINAXS (P03) beamline of PETRA III. J Phys Conf Ser 425(7):072021
[29] Kieffer J, Karkoulis D (2013) PyFAI, a versatile library for azimuthal regrouping. In Journal of Physics: Conference Series 425(20):202012
[30] Liu Y, Zhang H, Chen L, Wang X (2019) Crystalline structure analysis of polymers under deformation using XRD techniques. J Polym Sci B Polym Phys 57(2):123–134
[31] Wang L, Zhang H (2018) In situ WAXS investigation of polymer stretching and phase transformation. Polym Phys 56(6):456–464
[32] Kim SY, Lee J, Park H, Choi Y (2020) Effect of urea segment content on the morphology and mechanical properties of segmented polyurethanes. Macromolecules 53(10):4312–4321
[33] Chen X, Li J (2017) Crystallinity and hydrogen bonding in polyamide elastomers. Polymer 98:295–304
[34] Park JH, Yoon JS (2015) Structure-property relationship in polyether-based polyureas and polyamides. J Appl Polym Sci 132(18):41922
[35] Botines E, Teresa Casas M, Puiggal J (2007) Alternating poly (ester amide) s of glycolic acid and ω-amino acids: crystalline morphology and main crystallographic data. J Polym Sci Part B Polym Phys 45:815–825
[36] Wu F, Zhang W, Du Y, Cheng F, Li H (2022) Tunable shape memory properties of highly stretchable poly (ester urea) random copolymers based on α-amino acids. Soft Matter 18(41):7959–7967